What we want to know we can't measure

What we can measure we don't want to know

The power of isotope proxies…

"Non-traditional" Stable Isotope Systems

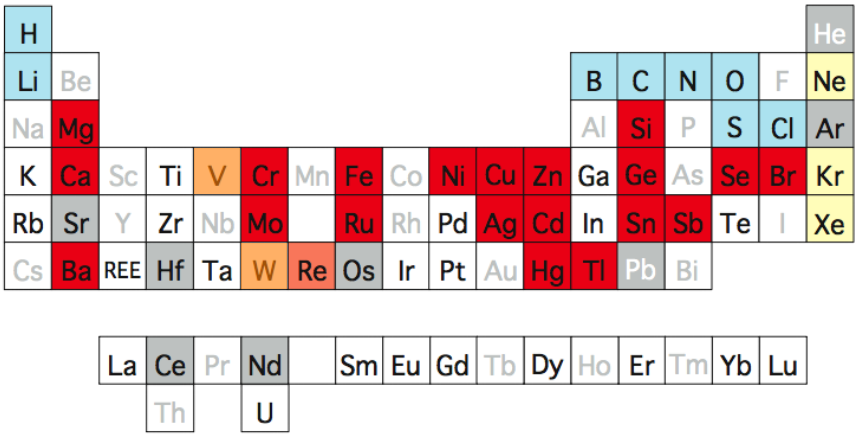

Qualitative Rules of Equilibrium Isotope Fractionation

Rule 1: Fractionation decreases with increasing temperature (T), for most substances ~$1/T^2$

Rule 2: Fractionation increases with decreasing mass (m) and increasing Δm ($m_{heavy} - m_{light}$), scaling approximately as $(m_{heavy} - m_{light})/(m_{heavy}m_{light})$

Rule 3: Heavy isotopes are concentrated in substances where that element forms the stiffest bonds (i.e., high spring constant, meaning short, strong chemical bonds)

Such bonds typically correlate with:

3.1: high oxidation state --- e.g., Fe^{3+} vs. Fe^{2+}

3.2: bonds to elements near the top of the periodic table

3.3: strongly covalent bonds (elements of similar electronegativity)

3.4: low-spin configurations in transition elements

3.5: low coordination number --- e.g., $B(OH)_3$ vs. $B(OH)_4^-$

Note: For heavy elements (~Mo-U) fractionations caused by changes in nuclear volume that increase (non-linearly) with mass can be larger than equilibrium effects and are largest when species with different s-orbital configurations equilibrate (e.g., Hg^0 [$6s^2$] vs. Hg^{2+} [$6s^0$]). These effects correlate with coordination number and the electronegativity of bond partners. Odd-even staggering in isotope abundance ratios results.

adopted from Schauble (2004/06)

Explanation to 3.4 (last slide)

Orbital energy gap (i.e., the geometry of ligand-electrons relative to the metal orbital) varies in magnitude depending on several factors, including the type of ligand. The Japanese chemistry R. Tsuchida devised the spectrochemical series from small Δ (i.e., energy gap) to large Δ values:

$I^- < Br^- < S_2^- < Cl^- < NO_3^-$, $N_3^- < F^- < OH^- < H_2O < NH_3 < NO_2^- < CN^- < CO$

Metal-ligand complexes with small Δ values (i.e., weak-field ligands) tend to form "high-spin" complexes (i.e. electrons fill the higher energy levels because the energy gap is small), whereas those with large Δ values (i.e., strong-field ligands) tend to form "low-spin" complexes (i.e., it is energetically favorable to fill the lower energy orbitals, even if that means pairing electrons). Low-spin implies the lowest number of unpaired electrons.

Ligand Field Theory works best for 1st row transition metals. Octahedral coordination (lining up of electrons with ligand orbitals) favors large energy splitting (strong field), whereas tetrahedral coordination favors lower energy splitting (weak-field).

Example #1:

Oxygenation of seawater

A molybdenum isotope perspective

Stable molybdenum isotope geochemistry

$\Delta m/m^2$ =~0.09%

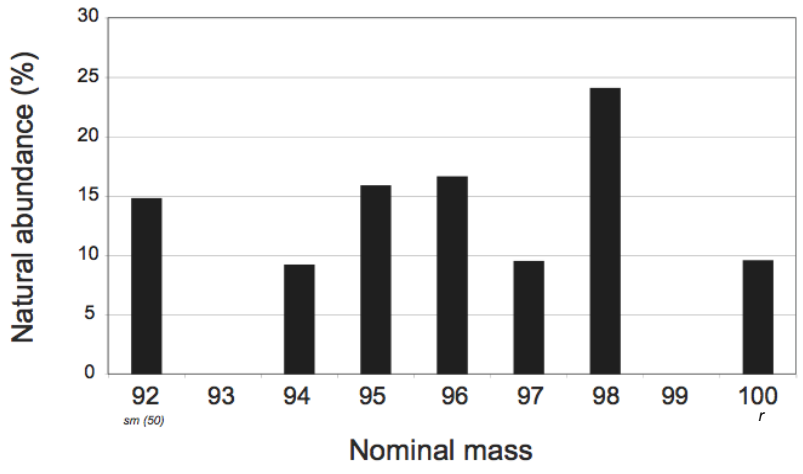

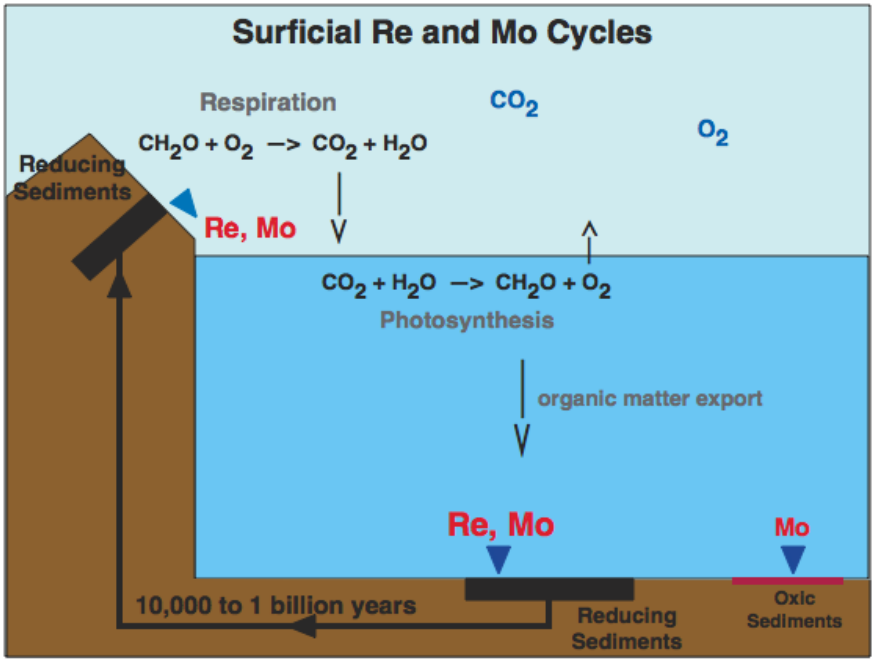

Two contrasting models for the evolution of atmospheric O_2

from Ohmoto, Geochem. News #93, Fall 1997

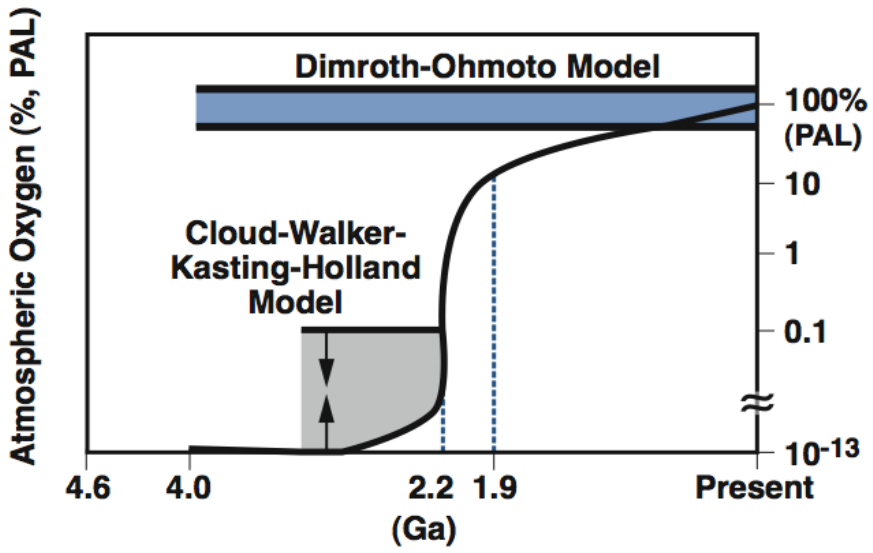

Remember…?

Proposed sequence of oxygenation of the atmosphere and ocean

from Ohmoto, Geochem. News #93, Fall 1997

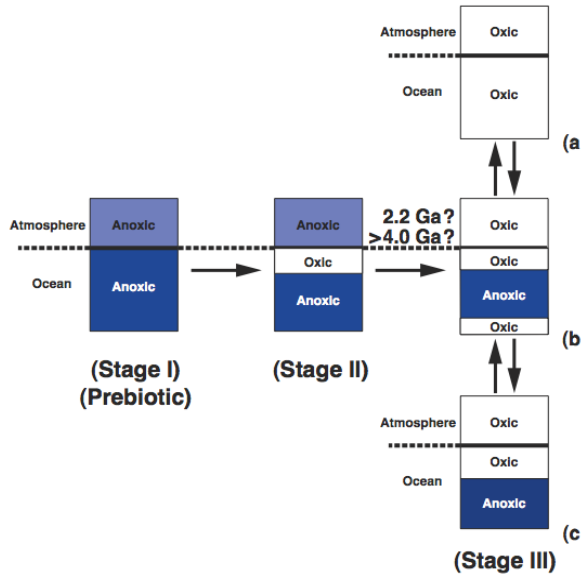

Natural fractionation of molybdenum isotopes

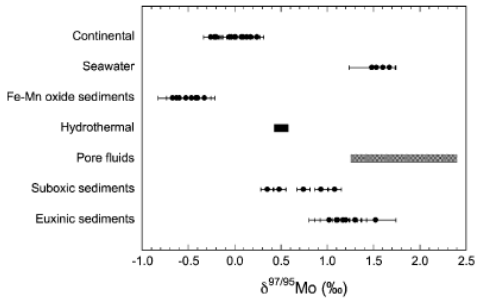

Fig. 1. Range of $\delta^{97/95}$Mo values observed in natural materials. Continental: granites, molybdenites, clastic marine sediments. Seawater: Atlantic, Pacific and Indian oceans. Fe–Mn oxide sediments: Atlantic, Pacific and Indian ocean ferromanganese crusts and nodules. Hydrothermal: end-member fluid composition inferred from data in low-*T* ridge flank system (100 km east of Juan de Fuca). Pore fluids: range of values in reducing porewaters from Santa Monica basin, <25 cm depth. Suboxic sediments: Santa Monica and San Pedro basins, Chile margin. Euxinic sediments: Cariaco basin and Black Sea. Uncertainties ±2σ. Data sources: [1–4].

Barling & Anbar, EPSL 217, 2004

Molybdenum isotopes of oxic marine deposits

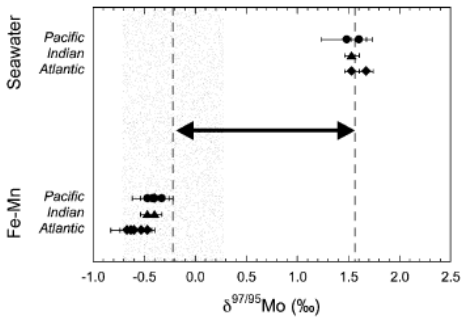

Fig. 4. Comparison of the isotopic offset between Mo in seawater and Mo in ferromanganese crusts and nodules expected from experimental findings with natural observations. The expected offset is derived from the mean seawater value (1.56‰) and $\alpha_{soln-MnOx} = 1.0018 \pm 0.0005$. The shaded region denotes the $\pm 2\sigma$ uncertainty on the expected value for adsorbed Mo. Observations are from Pacific (circles), Indian (triangles) and Atlantic (diamonds) oceans. Data sources as for Fig. 1.

Barling & Anbar, EPSL 217, 2004

Experimental oxic fractionation…

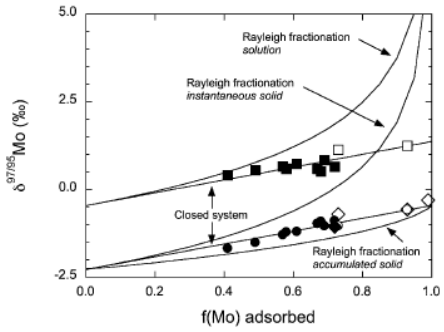

Fig. 6. $\delta^{97/95}Mo_{soln}$ and $\delta^{97/95}Mo_{MnOx}$ (both measured and inferred) versus fraction of Mo adsorbed by δ-MnO_2. Comparison of data with trends predicted for closed system equilibrium and Rayleigh fractionation models calculated using the experimentally determined $\alpha_{soln-MnOx}$. Time series experiments in closed symbols, pH series experiments in open symbols. For both series squares equal solutions, diamonds equal measured isotopic compositions of δ-MnO_2 and circles equal isotope compositions of δ-MnO_2 inferred by mass balance.

Barling & Anbar, EPSL 217, 2004

Molybdenum isotope paleo-redox-metry

Arnold et al., Science 304, 87-90, 2004; Barling et al., EPSL 193, 447-457, 2001.

Note the change in notation!

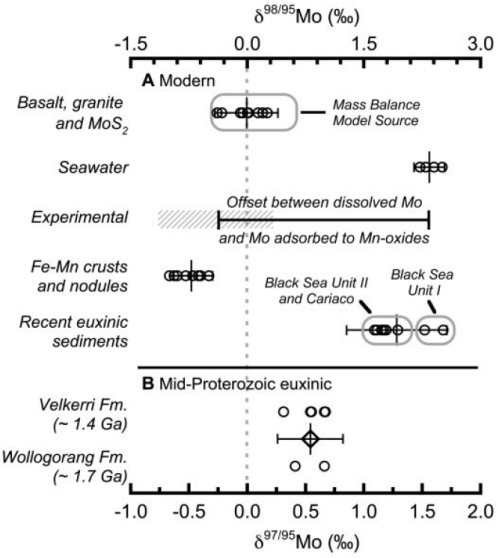

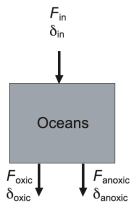

$$\Delta_{\text{sw-ox}} = \Delta_{\text{dissolved-adsorbed}} \approx 2‰$$

$$f_{\text{ox}} + f_{\text{eux}} = 1$$

$$\delta^{97/95}\text{Mo}_{\text{eux}} = \delta^{97/95}\text{Mo}_{\text{input}} + \Delta_{\text{sw-ox}} \times f_{\text{ox}}$$

Oxygenation of seawater after the GOE, ~2.3 Ga…

2-component system

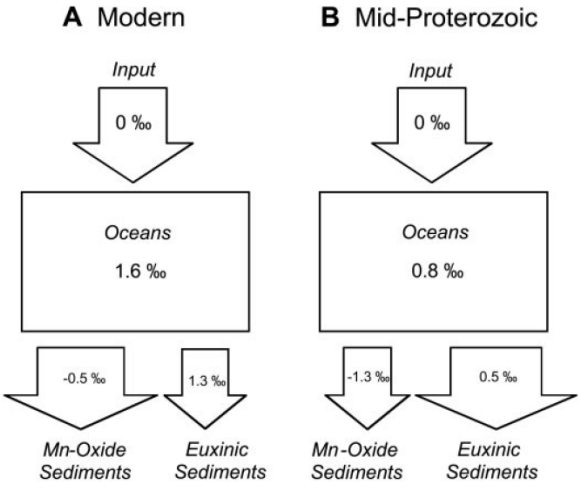

Fig. 2. Schematic depiction of Mo ocean isotope budget (**A**) today and (**B**) in the mid-Proterozoic, including average $\delta^{97/95}$Mo values for reservoirs, as indicated. Widths of arrows depict proportions of Mo removed to each sediment type. Offset between oceans and Mn oxides ($\Delta_{\text{sw-ox}} \approx 2$) is consistent with observations and laboratory experiments. Because of the possible importance of suboxic sediments to the Mo isotope budget in the mid-Proterozoic oceans, the proportion of Mo removed to Mn oxides may have been smaller than indicated in (B).

Arnold et al., Science 304, 87-90, 2004

Is it that simple? --- Some recent complications…

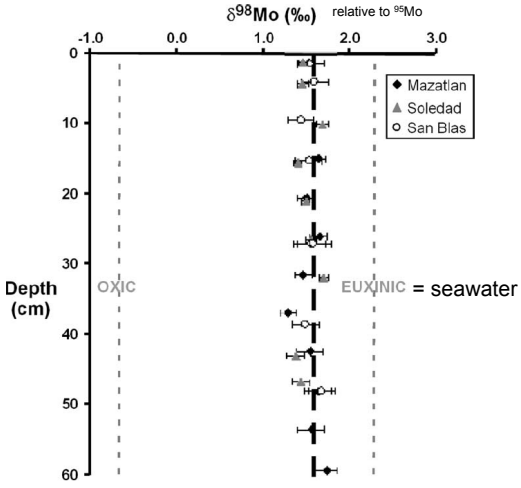

Figure 2. All δ^{98}Mo data (without lithogenic correction) from down-core profiles of the three anoxic Mexican margin sites in this study; errors shown are 2σ. The average Mo isotope composition of all measured samples is δ^{98}Mo = +1.6 ± 0.1‰ (1σ, n = 29) (Table 1).

Poulson et al., 2006

The role of suboxic marine environments…

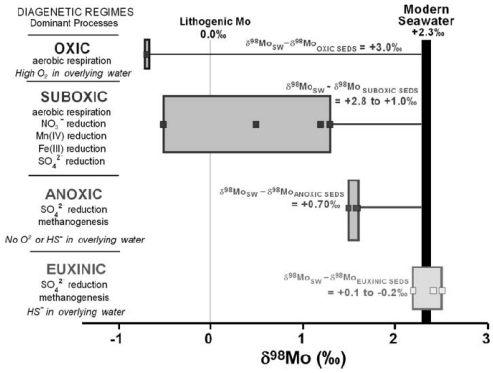

need for a 3rd component

Figure 1. Measured Mo isotope compositions of various marine sediments and the presumed dominant electron transport processes for each environment. Oxic sediment Mo isotope data are from Fe-Mn crust surfaces (Barling et al., 2001; Siebert et al., 2003). Suboxic sediment Mo isotope data are average site compositions from California margin sites of Siebert et al. (2006). Anoxic sediment Mo isotope data are average site compositions from three Mexican margin sites of this study. Euxinic sediment Mo isotope data are deep Black Sea sediments from Barling et al. (2001) and Arnold et al. (2004). All data are shown without lithogenic Mo correction.

Poulson et al., Geology 34, 617-620, 2006

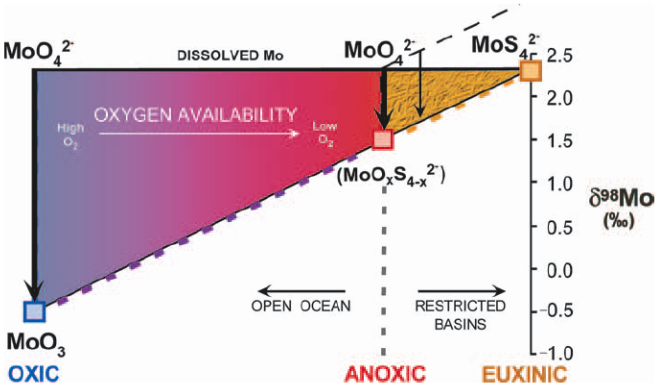

Figure 3. Schematic of the authigenic Mo isotope system in marine sediments depicting the measured oxic (δ^{98}Mo = −0.7‰), anoxic (δ^{98}Mo = +1.6‰), and euxinic (δ^{98}Mo = +2.3‰) Mo isotope signatures and proposed Mo chemical behavior. Measured Mo isotope compositions of marine sediments from open-ocean settings appear to reflect a mixture of lithogenic Mo (δ^{98}Mo = 0.0‰) and the authigenic Mo signature of either the oxic or anoxic Mo accumulation mechanisms. Measured Mo isotope values for restricted basin sediments suggest a change in the isotopic composition of dissolved Mo (dashed line at top) to heavier values as Mo is removed in the presence of dissolved sulfide.

Poulson et al., Geology 34, 617-620, 2006

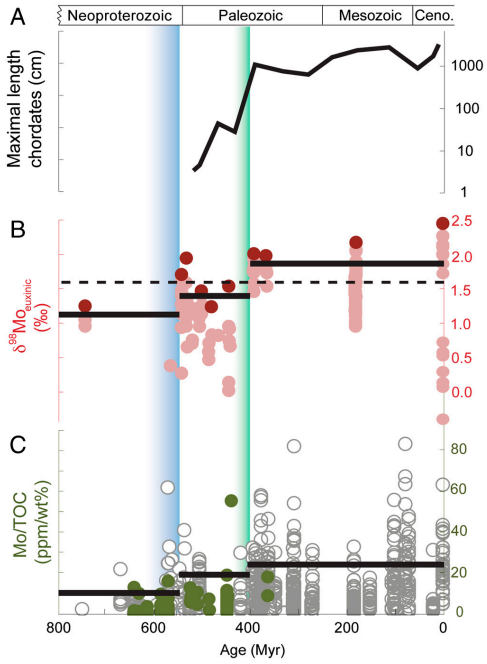

Mo isotopes in SW

Fig. 3. (*A*) Size maxima of vertebrates is used as a measure of maximal specific metabolic rate at a given time (42). (*B*) $\delta^{98}Mo_{SW}$ euxinic samples over the last 800 Ma with seawater value inferred from highly euxinic sediments (red circles) and mildly euxinic sediments fractionated to lower values (pink circles). Seawater values above the dashed line require a substantial oxic Mo sink. (*C*) Mo/TOC of black shales (new data, solid green circles; old data, gray circles; compilation summarized in SI Appendix). In *B* and *C* solid lines represent 90% percentiles for the three time periods: 800-542 Ma, 541-390 Ma, and 390-0 Ma. These three time periods are distinct from each other; see statistical analysis in *SI Appendix*. The Ediacaran emergence of large animals and the Devonian invasion of vascular land plants are shown by graded column bars in blue and green, respectively.

Dahl et al., PNAS 107, 42, 2010

A revised Mo isotope model (*3-components*)

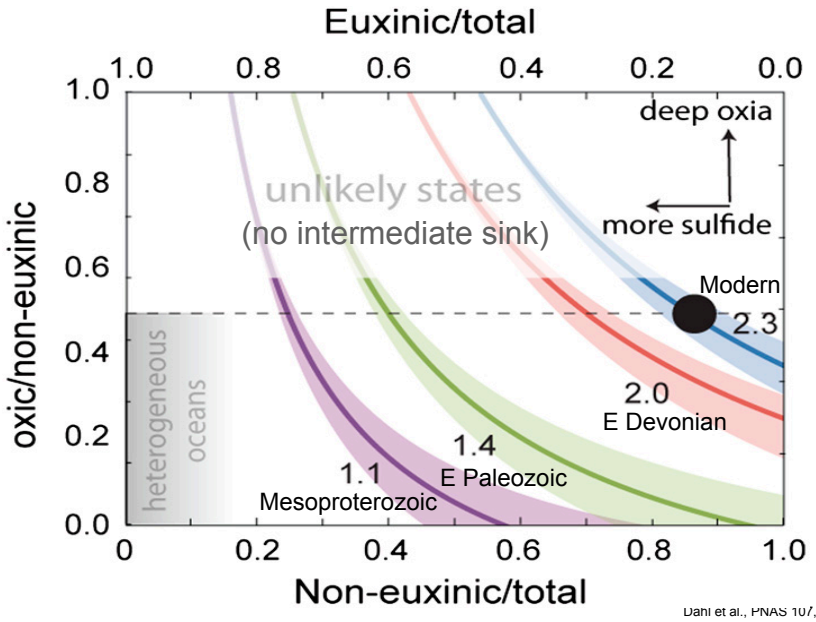

Dahl et al., PNAS 107, 42, 2010

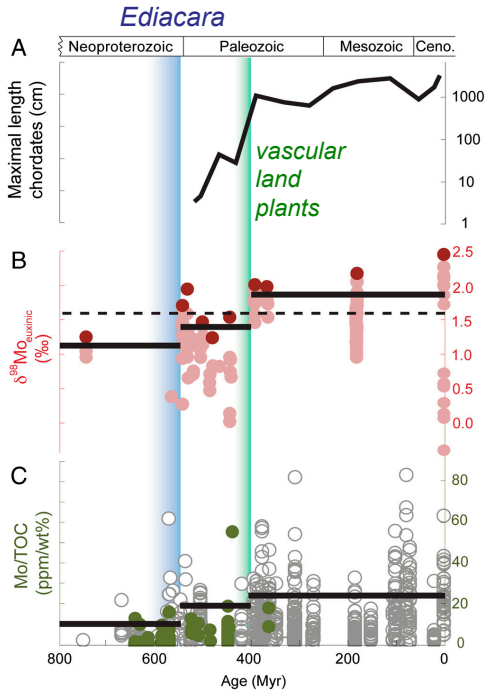

Mo isotopes

Ocean oxygenation

Evolution of life

Fig. 3. (*A*) Size maxima of vertebrates is used as a measure of maximal specific metabolic rate at a given time (42). (*B*) $\delta^{98}Mo_{sw}$ euxinic samples over the last 800 Ma with seawater value inferred from highly euxinic sediments (red circles) and mildly euxinic sediments fractionated to lower values (pink circles). Seawater values above the dashed line require a substantial oxic Mo sink. (*C*) Mo/TOC of black shales (new data, solid green circles; old data, gray circles; compilation summarized in SI Appendix). In *B* and *C* solid lines represent 90% percentiles for the three time periods: 800-542 Ma, 541-390 Ma, and 390-0 Ma. These three time periods are distinct from each other; see statistical analysis in *SI Appendix*. The Ediacaran emergence of large animals and the Devonian invasion of vascular land plants are shown by graded column bars in blue and green, respectively.

Dahl et al., PNAS 107, 42, 2010

Example #2:

Paleothermometry

A calcium isotope perspective

Title

from

Remember nucleosynthesis...?

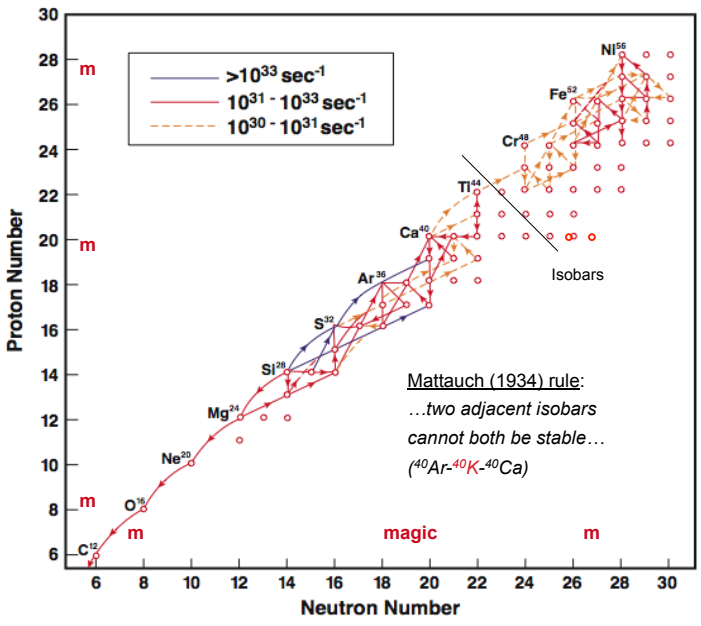

Stable calcium isotope geochemistry

$\Delta m/m^2$ =~0.4%

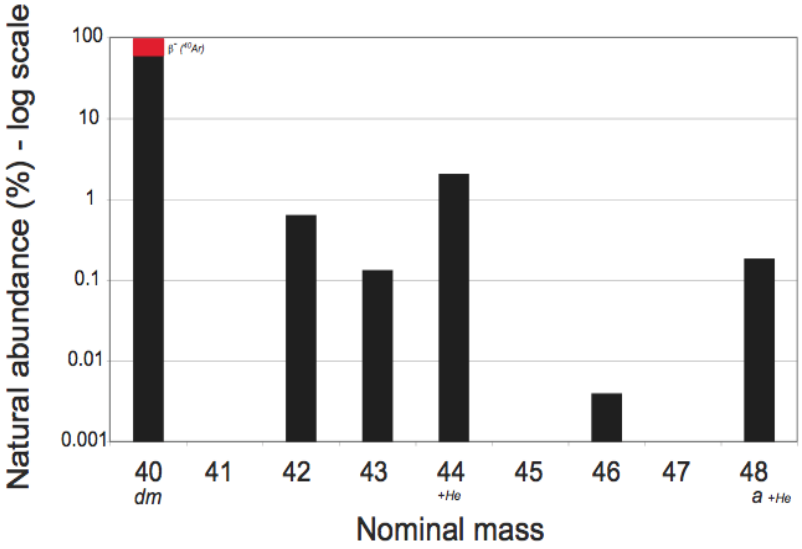

The importance of quantitative column yields...

Russel & Papanastassiou, Anal. Chem. 50, 1151-1154, 1978

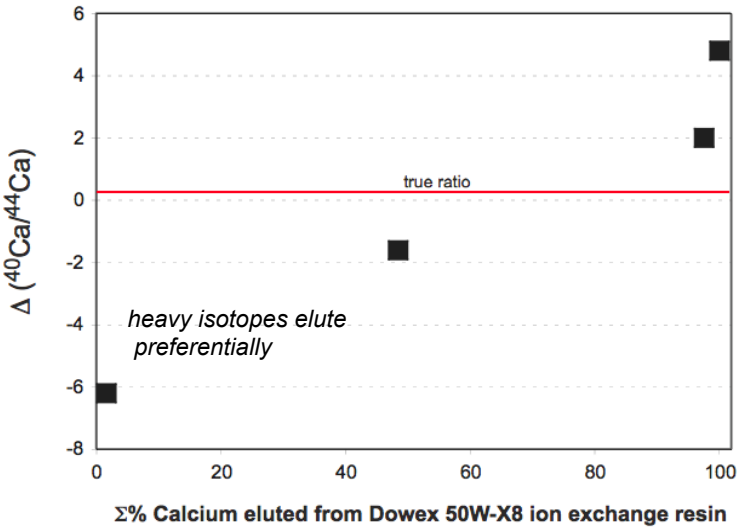

The Exploration Phase…

Table 6. Analytical results

Sample	Weight (mg)	Column Yield (Percent)	$(^{40}Ca/^{44}Ca)^{a}_{C}$	$\delta(^{40}Ca/^{44}Ca)$
Meteorites				
Abee-1 A (E4)	11	34	47.021±16	−2.8±0.4
			47.044±7	−2.3±0.1
Abee-1B	13[b]	SBC[c,d]	47.201±15	+1.0±0.3
			47.155±8	0.0±0.2
Abee-2A TR	12	96	47.143±7	−0.2±0.2
Abee-2B H_2O Leach[e]	25	83[f]	47.153±5	0.0±0.1
Norton County (aubrite)	21	SBC	47.193±6	+0.9±0.1
Orgueil (C1)	12	43[g,h]	47.166±6	+0.3±0.1
Guareña (H6)	50	56[h]	47.082±5	−1.5±0.1
Haverö (ureilite)	40	100[h]	47.122±6	−0.7±0.1
Ibitira (eucrite)	2	87[h]	47.146±9	−0.2±0.2
Lunar Samples				
70215	4	60-70[h]	47.103±8	−1.1±0.2
			47.108±5	−1.0±0.1
75055 Plagioclase	1	68[h]	47.126±8	−0.6±0.1
75055 Pyroxene	5	nm[i]	47.158±6	+0.1±0.1
15021-B Residue	9	62[h]	47.123±14	−0.7±0.3
15021-C Residue	106	SBC	47.181±9	+0.6±0.2
Terrestrial Samples				
Seawater	—	80-95	47.109±7	−1.0±0.2
		SBC	47.117±5	−0.8±0.1
Atlantic Ridge Tholeiite	8	nm	47.127±5	−0.6±0.1
Carbonatite (Tanzania)	5	nm	47.164±20	+0.2±0.4
Fluorite	3	96	47.165±10	+0.2±0.2
Calcite	4	87	47.123±6	−0.7±0.1
Thinolite-A	2	32	47.062±7	−2.0±0.2
			47.068±6	−1.8±0.1
Thinolite-B	17[b]	SBC	47.192±9	+0.8±0.2
Gypsum-1[j]	26	SBC	47.181±11	+0.6±0.2
Gypsum-2[k]	30	SBC	47.208±13	+1.2±0.3
Conch (*Strombus*) Seashell	7	95	47.170±6	+0.4±0.1
Chicken Eggshell	5	91	47.202±7	+1.0±0.2
Squirrel Tooth	36	>42[l]	47.240±14	+1.8±0.3
Shark Tooth, Mother (Root)[m]	2	SBC	47.193±6	+0.9±0.1
Shark Tooth, Fetus (Root)[n]	0.4	SBC	47.215±8	+1.3±0.2
Human Tooth (Root)	2	nm[o]	47.133±4	−0.4±0.1

Ca-isotope paleo-thermometry

Skulan et al., GCA61, 2505-2510, 1997; Zhu & Macdougall, GCA 62, 1691-1698, 1998; Nägler et al., G^3 1, 2000; and others

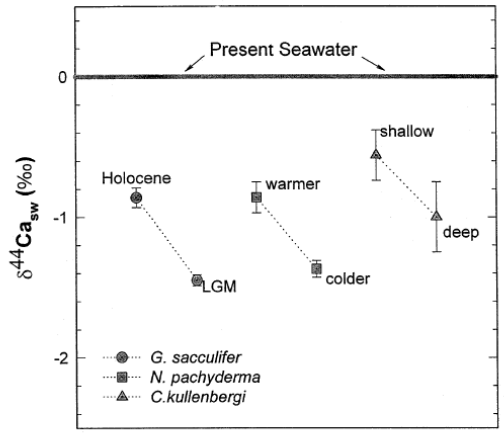

Fig. 2. Calcium isotopic data for three warm-cold pairs of foraminifera. Note that for each pair, both members are the same species. In each case, the colder individual of the pair is more highly fractionated from the seawater value. The data suggest that within a single species there may be systematic, temperature-dependent fractionation.

Ca isotope fractionation during carbonate precipitation

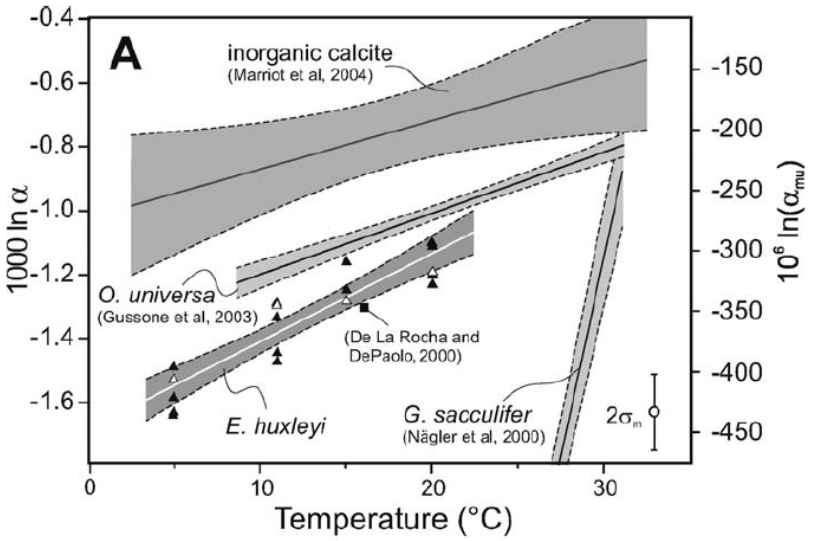

Ca isotope fractionation: calcite vs aragonite

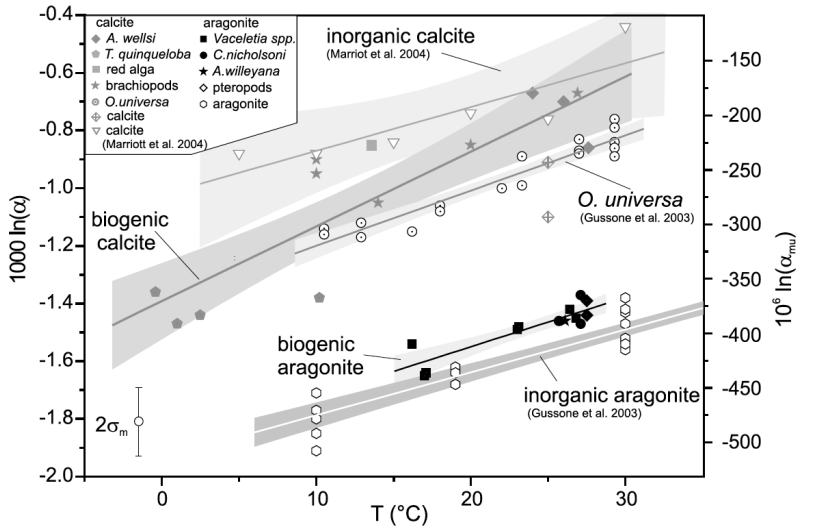

Fig. 1. Temperature dependent Ca isotope fractionation of different aragonitic and calcitic carbonates: aragonite samples (black symbols) are more enriched in ^{40}Ca than calcite samples (gray symbols). The offset is about 0.6‰ (150 ppm/amu). All fractionation-temperature trends have similar slopes of about 0.02‰/°C (5 ppm/amu · °C^{-1}).

Gussone et al., GCA 69, 4485-4494, 2005

The dependency of the Ca isotope fractionation factor on temperature and carbonate ion concentration

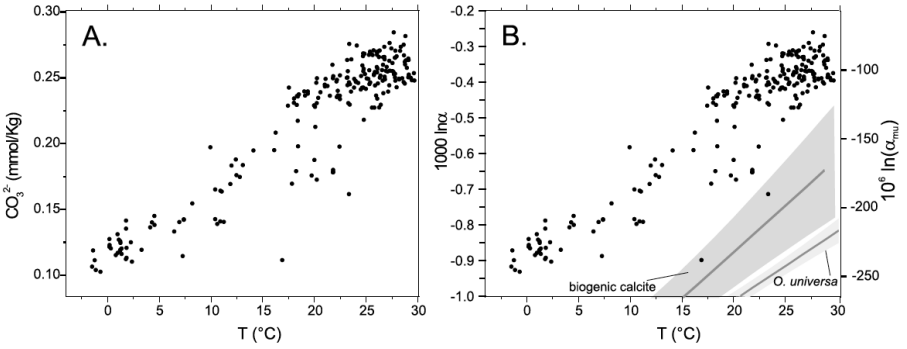

Fig. 2. (A) Carbonate ion (CO_3^{2-}) concentration in open ocean surface waters (0–50 m) as a function of temperature. The CO_3^{2-} concentration was calculated from DIC (dissolved inorganic carbon) and TA (total alkalinity) from GEOSECS data. (B) Calculated calcium isotope fractionation for calcite precipitated from waters with respective CO_3^{2-} concentration (after Lemarchand et al., 2004). The calculated 1000 · lnα values show a temperature dependence of 0.02‰/°C which is identical within error with the observed temperature calibration. There is an offset of about 0.5‰ between observed and calculated fractionation values.

Gussone et al., GCA 69, 4485-4494, 2005

The role of calcification rate…

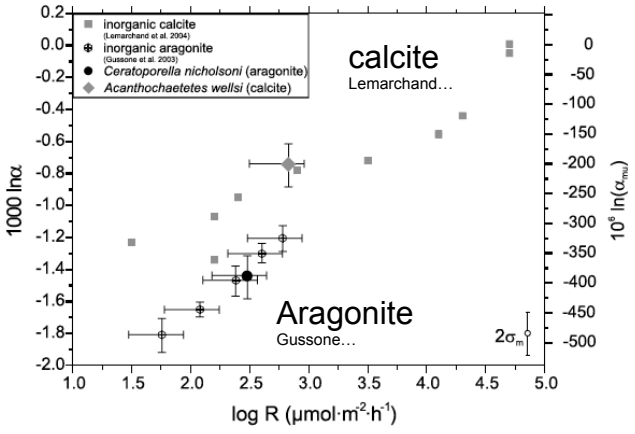

Fig. 3. Calcium isotope fractionation (1000 · lnα) as a function of the precipitation rate (μmol · m^{-2} · h^{-1}). The offset between calcite and aragonite at the same precipitation rate is about 0.6‰ (150 ppm/amu). Horizontal error bars indicate ±50% variation of the precipitation rates.

Gussone et al., GCA 69, 4485-4494, 2005

The effect of carbonate-ion concentration…

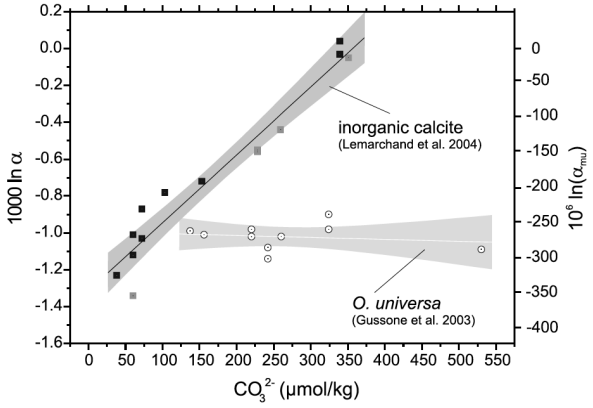

Fig. 4. Calcium isotope fractionation ($1000 \cdot \ln\alpha$) of *O. universa* (Gussone et al., 2003) and inorganically precipitated calcite (Lemarchand et al., 2004) as a function of CO_3^{2-}. Inorganic calcite shows a strong decrease of Ca isotope fractionation (increasing $1000 \cdot \ln\alpha$) with increasing carbonate concentration, while the planktonic foraminifer *O. universa* shows no significant variation.

How does the planktonic foraminifera *Orbulina universa* regulate its Ca-uptake?

Gussone et al., 2005

pH and $[CO_3]^{2-}$ dependency…

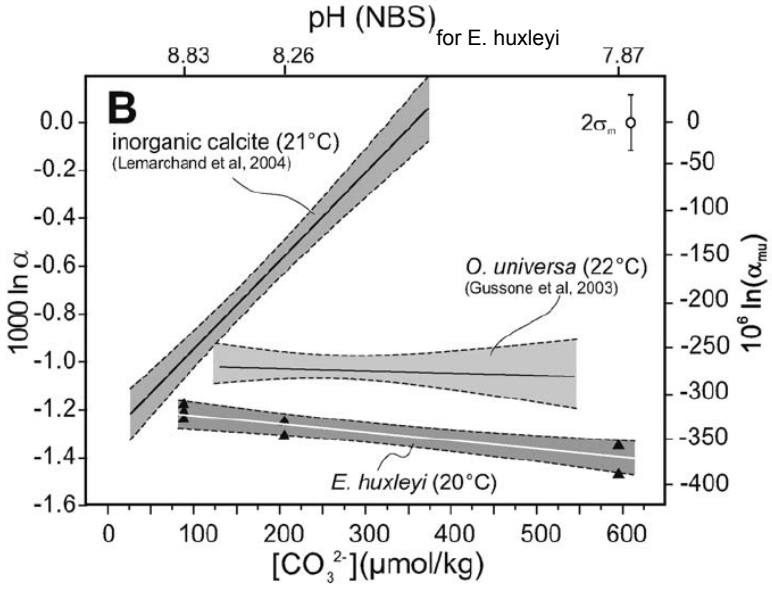

Thoughts on how Ca makes it from seawater

into the biogenically formed carbonate

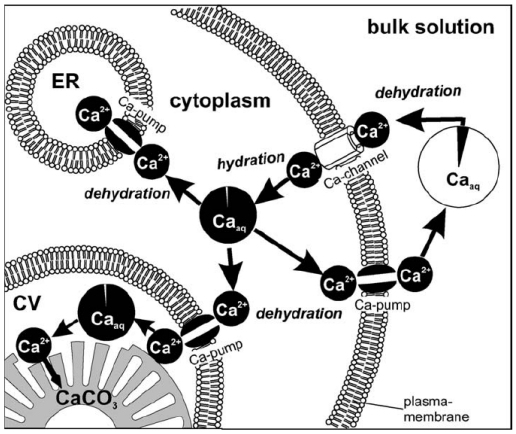

Ca in seawater exists as a large, hydrated aqua-complex (large mass, low $\Delta m/m^2$)

Figure 2. Proposed calcium transport pathways in *Emiliania huxleyi* from seawater to site of calcification: Dissolved Ca (Ca_{aq}) is dehydrated at cell surface and transported through Ca-selective channels into cell. Ca^{2+} ion that enters cytoplasm is rehydrated and removed from cytoplasm by Ca pumps and transferred into cell organelles (e.g., endoplasmic reticulum [ER] or Golgi apparatus), in coccolith vesicle or out of cell. Ca entering coccolith vesicle (CV) is nearly completely incorporated into $CaCO_3$ of coccolith. Calcium reservoirs are shown as pie charts, and dimension of black pie slice indicates portion of Ca removed from respective Ca reservoir (not to scale).

Example #3:

Long-term climate and the carbon cycle

A calcium isotope perspective

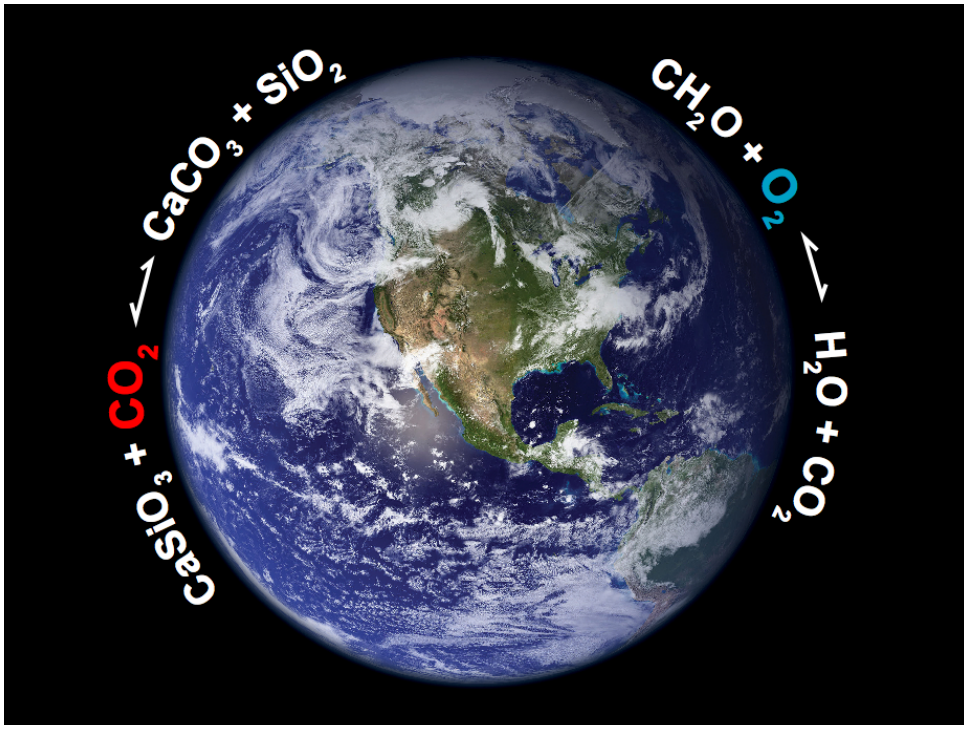
$CaSiO_3 + CO_2 \rightleftharpoons CaCO_3 + SiO_2$
$CH_2O + O_2 \rightleftharpoons H_2O + CO_2$

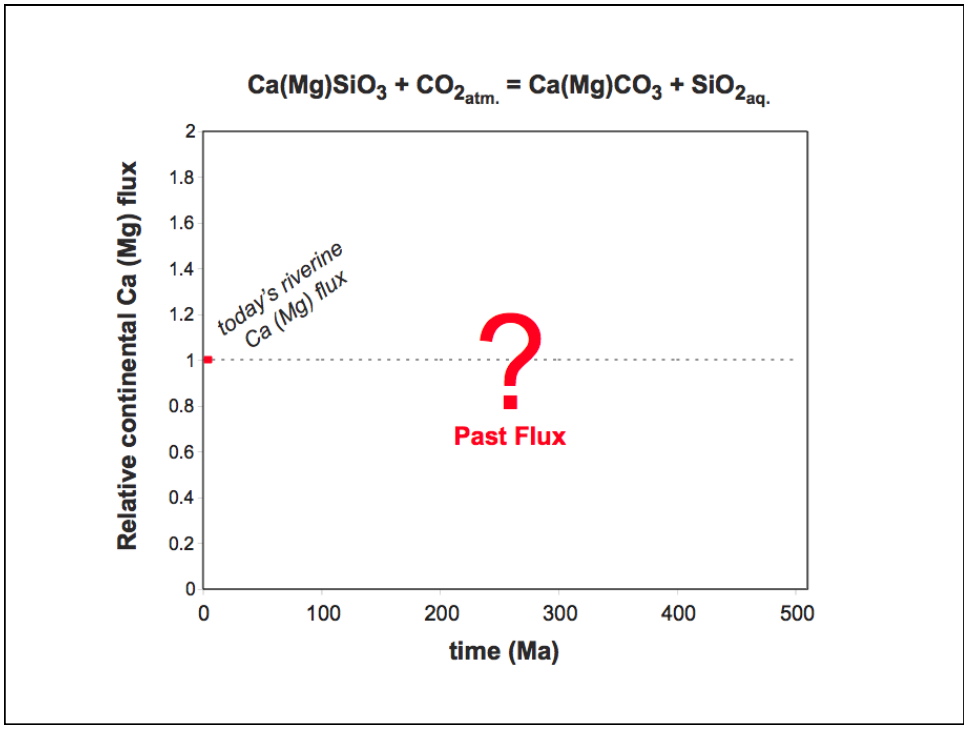
$Ca(Mg)SiO_3 + CO_{2atm.} = Ca(Mg)CO_3 + SiO_{2aq.}$
Relative continental Ca (Mg) flux
2
1.8
1.6
1.4
1.2
1
0.8
0.6
0.4
0.2
0
today's riverine Ca (Mg) flux
?
Past Flux
0
100
200
300
400
500
time (Ma)

The marine Ca isotope system

Zhu & Macdougall, GCA 62, 1691-1698, 1998

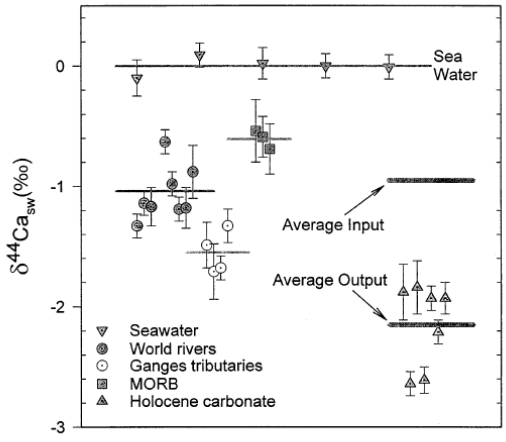

Fig. 1. Summary of Ca isotopic data for the oceanic Ca cycle. Average values are shown as thin shaded lines for seawater, MORB, Ganges tributaries, and the other rivers we have measured. The average output value is calculated from the data for Holocene coral and carbonate ooze, and the average input from MORB (≡ hydrothermal) and river data as explained in the text. The Ganges tributary data are not included in the input average.

The marine Ca isotope system

Zhu & Macdougall, GCA 62, 1691-1698, 1998

$$N_{Ca}\, d\delta^{44}Ca_{sw} / dt = F_{river}\,(\delta^{44}Ca_{river} - \delta^{44}Ca_{sw}) + F_{hydro}\,(\delta^{44}Ca_{hydro} - \delta^{44}Ca_{sw}) - F_{sed}\,\Delta_{sed}$$

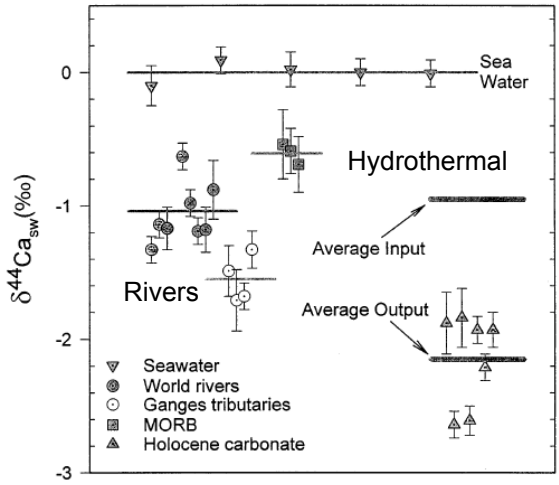

$- F_{sed}\,\Delta_{sed}$

Ca isotope variations of seawater

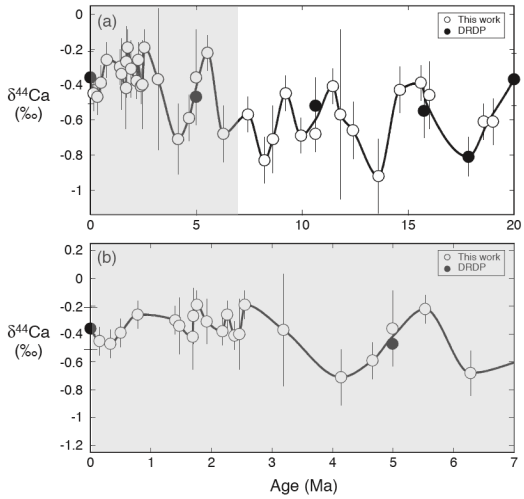

Fig. 1. The calcium isotope record based on data from DSDP Hole 590B (○) and De La Rocha and DePaolo (DRDP; ●) [9]: (a) the entire 20 million year period sampled in the study and (b) a blow-up of the period between 0 and 7 Ma, for which we have particularly dense sampling between ~1.5 and 2.5 Ma. Error Bars (2σ) are indicated for all samples.

Fantle & DeDaolo, EPSL 237, 102-117, 2005

Ca flux from weathering vs sedimentation

Fantle & DePaolo, EPSL 237, 102-117, 2005

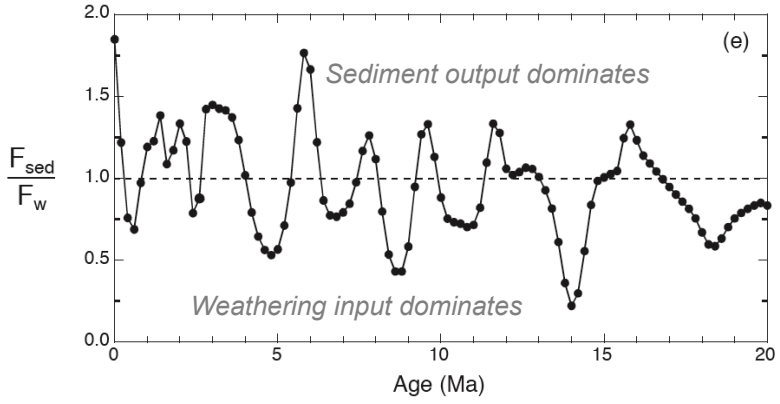

$$\frac{F_{\mathrm{Sed}}}{F_{\mathrm{W}}} = \frac{1}{\Delta_{\mathrm{Sed}}}\left[\frac{N_{\mathrm{Ca}}}{F_{\mathrm{W}}}\frac{\mathrm{d}\delta_{\mathrm{SW}}}{\mathrm{d}t} + (\delta_{\mathrm{W}} - \delta_{\mathrm{SW}})\right]$$

$\delta_{\mathrm{W}} = -0.48$

$\delta^{44}\mathrm{Ca}$ (‰) of seawater ($=\delta_{\mathrm{carb}} + 1.3$‰)

Good books…

- *Geochemistry of non-traditional stable isotopes*, Clark Johnson, Brian Beard, Francis Albarède (Eds.), Rev. Mineral. & Geochem. 55, 2004.

- *Principles of stable isotope distribution*, Robert Criss, Oxford Univ. Press, 1999.